Fatigue Behavior of Engineering Polymers and Its Numerical Implementation

Pieter Volgers[1], Amir K. Shojaei[2]

DuPont Transportation and Advanced Polymers
[1]European Technical Center, Switzerland; [2]Chestnut Run Plaza, Wilmington, DE.

Abstract: *DuPont's engineering polymers are used in a wide range of applications and industries. Many of these parts, from engine mounts to gears, are subjected to fatigue loading. Accurate prediction of their fatigue performance in real-life conditions is therefore important to prevent either premature failure or over-designing of the component. However, material fatigue data available following standard testing is not automatically representative of the actual conditions. In addition to this, available software tools, such as fe-safe, do not capture all the phenomena observed in engineering polymers, most specifically the effects of self-heating. These effects can have a significant influence in the fatigue performance.*

As a material supplier, it is our role to understand the behavior and performance of our materials and to support designers and engineers in their optimal use. In this paper we will describe the material behavior of semi-crystalline engineering polymers, illustrated with material test data on Delrin® POM and their influence on their fatigue performance, in particular their non-linear elastic (hyperelastic) response, hysteresis, temperature dependence and self-heating effects. These have been included in an in-house tool based on Abaqus for improved prediction of the fatigue performance of engineering polymer parts in real-life conditions.

Keywords*: Constitutive Model, ,Fatigue, Fatigue Life, Polymer, Viscoelasticity.*

1. Introduction

Many structural components are subjected to cyclic loading, whereby the lifetime is determined by the material fatigue. Accurate prediction of the fatigue performance can prevent premature failure, or over-dimensioning of the part. Fatigue prediction methods are well-established for metals and are generally extended for application to engineering polymers. However, it is well known that polymers behave differently from metals, particularly showing a viscoelastic response. It is therefore logical to conclude that the fatigue prediction will have to include the specific effects related to engineering polymers.

The objective of this paper is to describe the material mechanical behaviors of engineering polymers considered relevant to their fatigue behavior. These phenomena have been implemented using in-house user subroutines in Abaqus for improved fatigue prediction. The results of this tool will be presented.

Many investigations into the behavior of semi-crystalline thermoplastic polymers are based on the testing of polyamides (e.g. Ghorbel, 2008, Ghorbel et al., 2014, Maurel-Pantel et al, 2015). For practical purposes of this paper, we will use DuPont™ Delrin® POM homo-polymer as an example. Delrin® is mostly used without fillers or reinforcements, its glass transition temperature is at -20°C, so that for most practical applications we do not have to deal with effects of passing the glass-transition temperature T_g, and is used in a wide range of applications where fatigue is an important aspect of the design, from gears to snap-fits and conveyor belts.

2. Material behavior

The basic material behavior of Delrin® has been presented at the Science in the Age of Experience Conference in 2017 (Volgers et al., 2017), some of which will be repeated here for completeness.

2.1 Static cyclic loading

Standard published material stress-strain data, as found in the CAMPUS database[1], has been tested following the ISO 527-1 and -2 standards. The continuous loading conditions defined in these standards do not allow any determination of permanent deformation. Common industry use is to assume a classical elastic-plastic material model, but cyclic loading clearly shows the non-linear constitutive behavior, as shown in Figure 1.

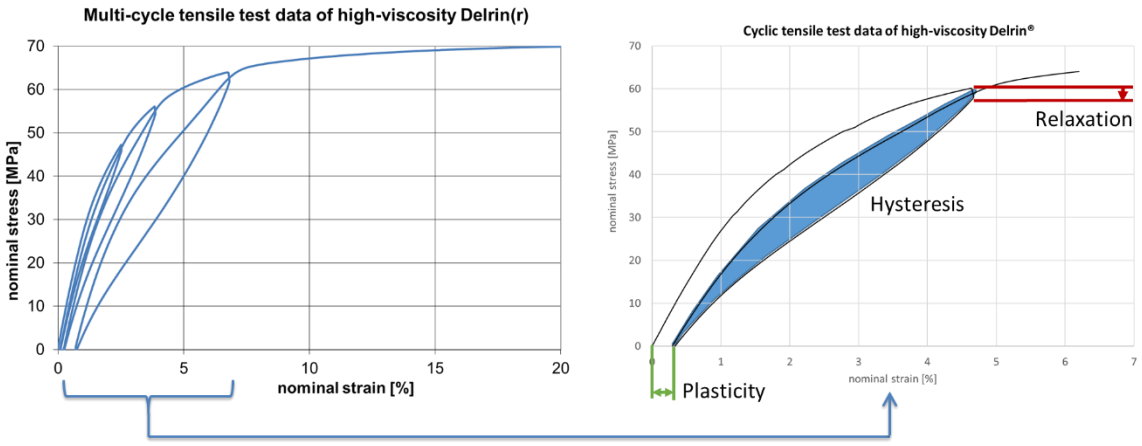

Figure 1: Cyclic tensile test data (room temperature)

A close-up of the test data shows some of the behavior which may have to be considered depending on the load case and the needs of the analysis. During the short transition period where the static tensile testing machine switches the loading direction, initial stress relaxation is already

[1] CAMPUS: Computer Aided Material Preselection by Uniform Standards. http://www.campusplastics.com/

visible in the measured force-displacement curve (shown as stress-strain). Despite the stress level being well into the non-linear domain, the amount of plastic deformation is very small, demonstrating the hyperelastic behavior of the material. And the reloading response does not follow the unloading response, but shows a certain amount of hysteresis. These effects may or may not be relevant for the structural analysis, although the use of a hyperelastic material model is highly recommended for strains beyond 1%, even in monotonous quasi-static loading (see Shojaei, 2018; Volgers, 2017).

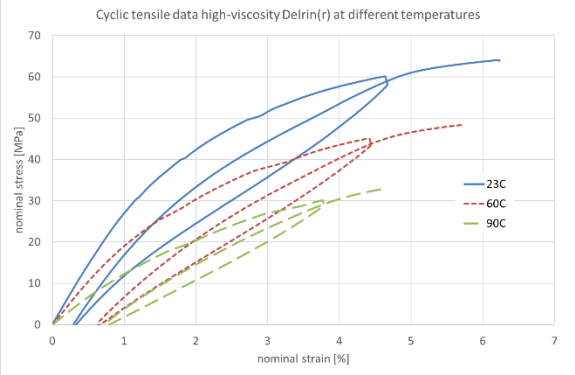

Figure 2: Temperature dependence of cyclic response

Increased temperature reduces the stiffness of thermoplastic polymers. Cyclic testing of the material at elevated temperatures also shows the increase of plastic deformation but with reduced hysteresis, as seen in Figure 2.

2.2 Viscoelastic response

The cyclic quasi-static cyclic tensile testing results shown in the previous section already indicated a significant viscous behavior when changing from loading to unloading of the testing machine. More information can be obtained by stress-relaxation measurements and short-term creep testing.

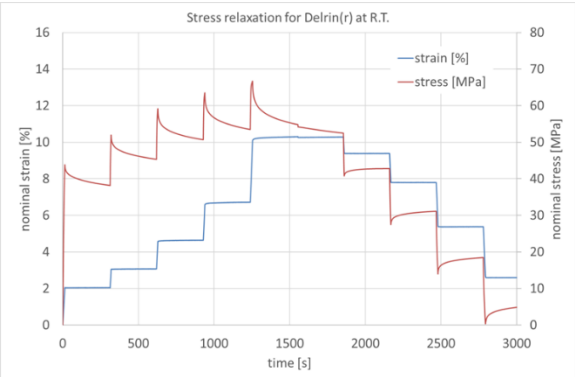

Figure 3: Short-term stress-relaxation – stress and strain over time

Incremental stress-relaxation testing as shown in Figure 3 and Figure 4, is done by increasing the strain to a pre-defined level and then maintaining this strain level for a certain period of time before increasing the strain again.

Figure 3 shows both the stress and the strain over time, whereby the strain is increased step-wise up to 10% strain, after which the stress level is reduced step-wise until initial zero-stress has been reached. For each increase of the strain, the stress increases accordingly, while quickly reducing by about 10% over 5 minutes, before increasing again. The inverse effect is observed in the unloading steps.

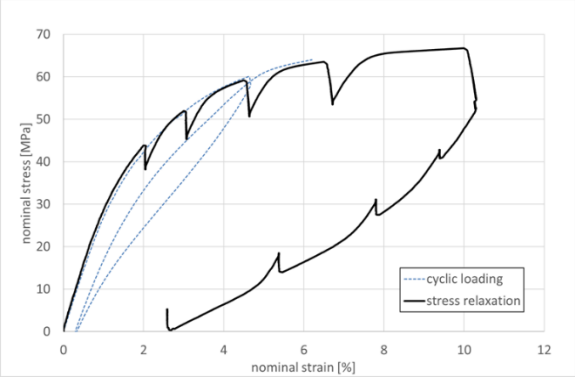

Figure 4: Short-term stress relaxation - stress vs strain

Figure 4 shows the same data, but in stress versus strain. In dashed blue is the cyclic stress-strain response (at room temperature) from Figure 2, providing a perfect match to the outer curve of the stress-relaxation curve, despite the intermediate relaxation phases.

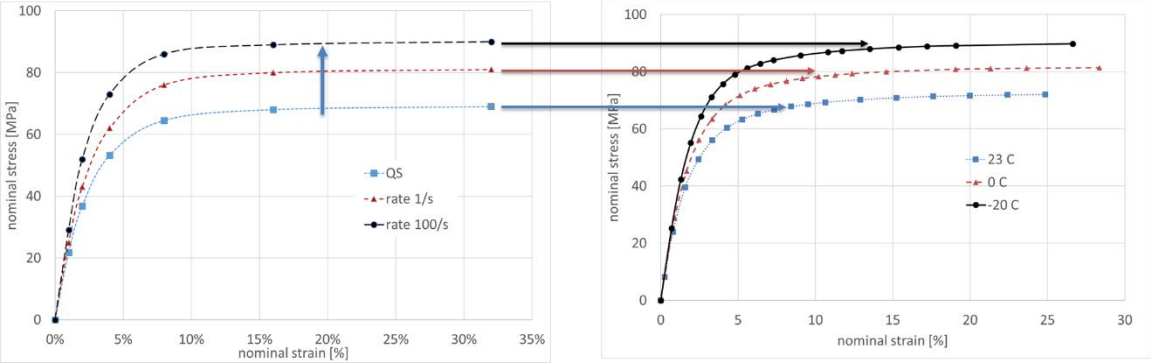

Figure 5: Strain-rate dependence and temperature equivalence

The visco-elastic response shown would indicate a strain-rate dependency. On the left of Figure 5 this dependency is clearly shown. The increasing strain rate has hardly any influence on the initial

stiffness response, but increases the non-linear part of the curve, increasing the stress level with increasing strain rate with about 30%.

The main strain-rate dependent curves can be related to the performance at different temperatures, as shown in Figure 5 on the right. This time-temperature relationship can be used inversely to predict the behavior at increasing strain-rate by reducing the temperature instead of increasing the strain rate. (e.g. Maurel-Pantel et al, 2015).

3. Fatigue testing

The quasi-static and dynamic material behavior provide the basics for the modelling of its fatigue behavior. To support the fatigue analysis, a detailed series of fatigue tests has been performed on a single machine, to reduce the effect of machine variability. An electric-controlled state-of-the-art testing machine was used. In order to better include the material temperature dependence, fatigue tests were performed at room temperature, 40°C and 60°C with and R-value of 0.1 and a frequency of 10 Hz, as commonly used.

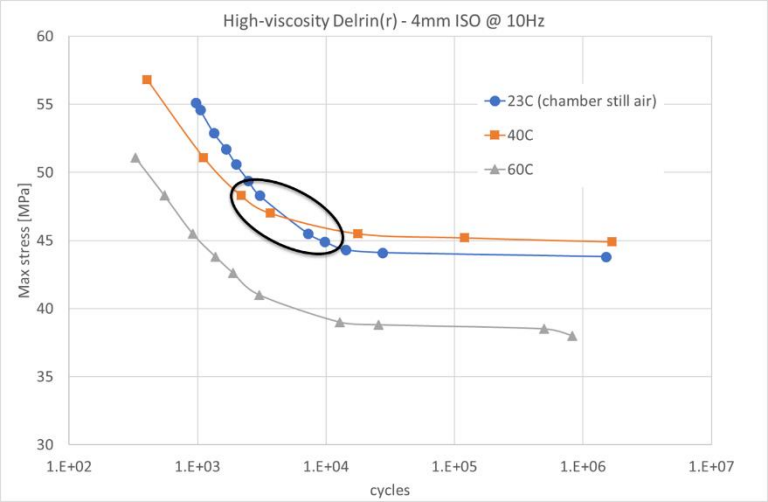

Figure 6: Standard fatigue testing results at different temperatures

Figure 6 shows the test data as obtained with the new equipment with high repeatability of the test results. Most notably in the data as shown above is the cross-over of the graphs for 23°C and 40°C at around 47 MPa. This would indicate that the material performs better at 40°C than at room temperature for cyclic loading of 10'000 cycles or more, which does not fit with standard considerations on the evolution of fatigue damage and failure.

Further consideration of the testing method concluded that, for the fatigue testing at elevated temperatures the temperature chamber maintained its set temperature by circulating the air in the test chamber, while the room temperature testing was done with the chamber door open, which assumed that the laboratory temperature (23°C) was maintained for the air around the sample. It

was therefore decided to create the same air conditions for the room temperature testing as for the elevated temperature testing, by closing the testing chamber and circulating the air in the same manner to maintain a chamber temperature of 23°C. The results are shown in Figure 7 below.

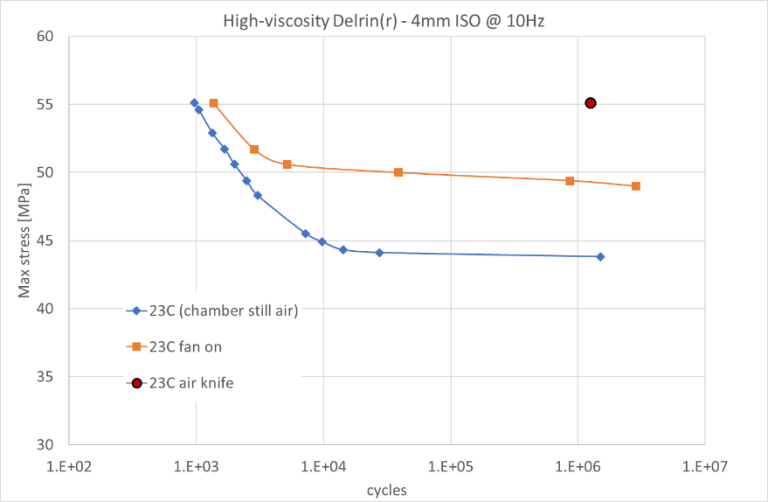

Figure 7: Fatigue test results for different temperature controls (23°C)

Apparently, the circulating air has a cooling effect on the sample, thereby significantly increasing the fatigue performance of the material. An additional test was performed whereby the test sample was actively cooled with an air knife at a temperature of 23°C, with the additional data point shown in Figure 7 at the upper right corner.

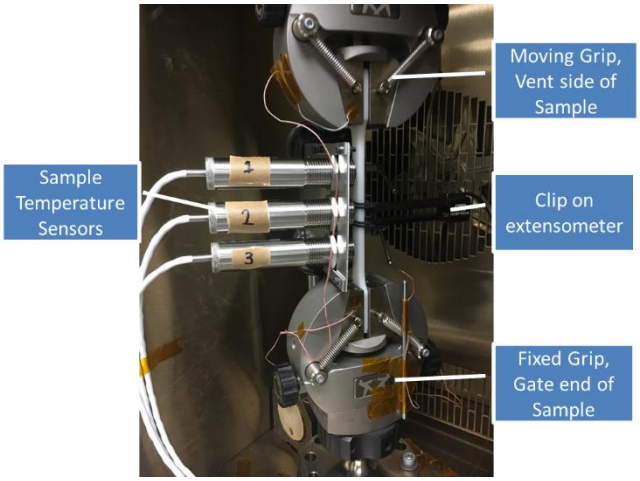

Figure 8: Fatigue testing set-up with temperature sensors

To further investigate the temperature situation of the fatigue test, temperature sensors were installed to monitor the actual temperature at 3 different positions on the specimen, as shown in Figure 8. The temperature recordings for different fatigue performances are shown in Figure 9 and Figure 10 below.

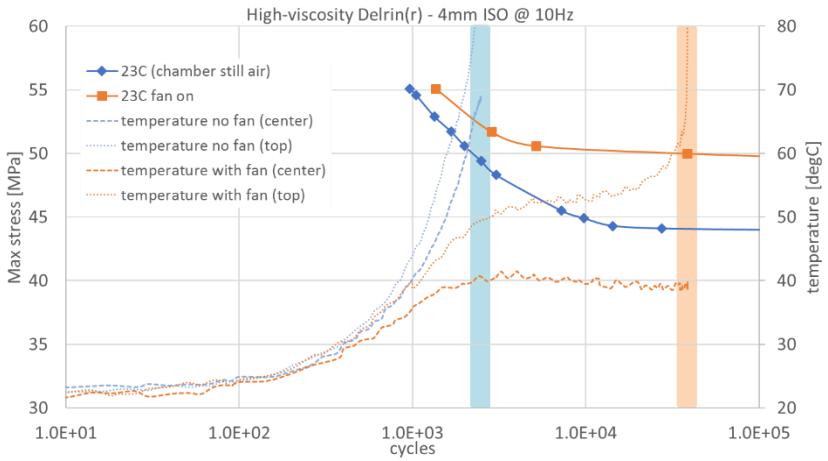

Figure 9: Temperature measurements at fatigue sample testing around 50 MPa.

When looking at the temperature readings at the central and top sensor for fatigue tests with a peak stress of about 50 MPa (49.4 MPa for the test in still air, 50MPa for the test at circulating air), we observe a continuous increasing temperature at the sample in still air, up to 70°C in the center, until failure occurs at about 2500 cycles. The center readings for the specimen in circulating air stabilize around 40°C, while the top reading goes to slightly over 50°C until it peaks at the moments of specimen failure in a run-away temperature.

Another way of looking at the temperature effects is by considering the temperature profiles for two data points with the same number of cycles to failure. To reach a fatigue failure limit of about 30’000 cycles (10 Hz, R=0.1), the sample in the still air is loaded to a peak stress of 44 MPa, while the sample in the circulating air can be loaded to a peak stress of 55 MPa.

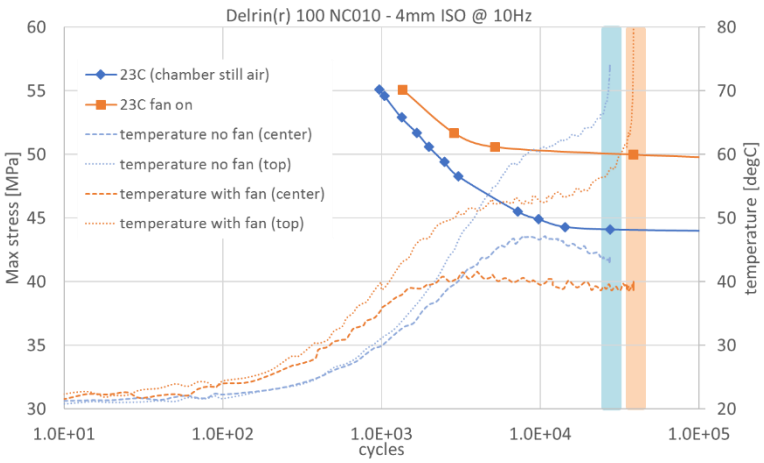

Figure 10: Temperature measurements at fatigue sample testing around 30k cycles

The temperature measurements clearly show the actual temperature increase in the test samples and the difference due to the air circulation. While the still air allowed the center section of the sample to reach almost 50°C, the upper sensor measured a temperature exceeding 60°C, before a temperature run-away event occurred at the moments of failure. The sample temperature in the circulating air is limited to 40°C in the center section and slightly above 50°C for the top sensor, before the same temperature run-away effect is observed at the moments of failure.

4. Implementation in Abaqus

Based on static analysis and corresponding material laws, as visco-elastic behavior requires dynamic analysis. Temperature dependence included initially in material model parameters for elastic-plastic behavior, currently in the calibration of the damage behavior. The method is implemented in Abaqus using user-defined routines and described in detail in (Shojaei and Volgers, 2018), of which below is an abbreviated version.

4.1 Kinematics

Static material testing (Section 2.1) has shown the non-linear elastic behavior of the polymer. The benefits of using a hyperelastic model for Delrin® has been shown in (Volgers and Winkler, 2017; Shojaei and Volgers, 2018) and have been included in the fatigue analysis. The first order Mooney-Rivlin (MR) model (Mooney, 1940; Ogden, 1972) provides enough accuracy for capturing both loading and unloading response of engineering polymers

$$W = C_{01}(\bar{I}_2 - 3) + C_{10}(\bar{I}_1 - 3) + D_1(J-1)^2$$

where C_{01} and C_{10} are material constants elated to the distortional response and D_1 is a material constant related to the volumetric response, $\bar{I}_1 = J^{-2/3}I_1$, and $\bar{I}_2 = J^{-2/3}I_2$ with I_1 and I_2

indicating first and second invariants of the left Cauchy-Green **elastic** deformation tensor, and $J = \det(F_{ij}^e)$. For consistency with linear elasticity in the limit of small strains, it is necessary that

$$D_1 = K/2 \text{ and } C_{01} + C_{10} = \mu/2$$

where K is the *damaged* bulk modulus and μ is the *damaged* shear modulus of the solid, to be defined further below. The Cauchy stress in a compressible hyperelastic material with a stress-free reference configuration is given by:

$$\sigma_{ij} = \frac{2}{J}\left[\frac{1}{J^{2/3}}\left(\left(\partial W/\partial \bar{I}_1\right) + \bar{I}_1\frac{\partial W}{\partial \bar{I}_2}\right)B_{ij} - \frac{1}{J^{4/3}}\left(\frac{\partial W}{\partial \bar{I}_2}\right)B_{ik}B_{kj}\right] + \left[\frac{\partial W}{\partial J} - \frac{2}{3J}\left(\bar{I}_1\frac{\partial W}{\partial \bar{I}_1} + 2\bar{I}_2\frac{\partial W}{\partial \bar{I}_2}\right)\right]\delta_{ij}$$

where δ_{ij} is the Kronecker delta and B_{ij} is the left Cauchy–Green deformation tensor.

$$C_{10} = \frac{\partial W}{\partial \bar{I}_1}, C_{01} = \frac{\partial W}{\partial \bar{I}_2}, 2D_1(J-1) = \frac{\partial W}{\partial J}$$

Based upon small deformation assumption and following (Chaboche, 1991; 1997; 2008), Chaboche's plasticity flow rule with kinematic and isotropic hardening is utilized to capture cyclic loading responses in unfilled polymeric system:

$$\dot{\epsilon}_{ij}^p = \frac{3}{2}\left|\dot{\epsilon}_{ij}^p\right|\frac{s_{ij}^*}{\sigma_y}$$

where $\left|\dot{\epsilon}_{ij}^p\right| = \sqrt{\frac{2}{3}\dot{\epsilon}_{ij}^p\dot{\epsilon}_{ij}^p}$ is the effective plastic strain rate and σ_y is the yield stress. The deviatoric stress s_{ij}^* is computed based on the following relation [35]

$$s_{ij}^* = s_{ij} - X_{ij}$$

where $X_{ij} = \alpha_{ij} - \frac{1}{3}\alpha_{kk}\delta_{ij}$ is the deviatoric part of the backstress tensor α_{ij} (to be defined later), and $s_{ij} = \sigma_{ij} - \frac{1}{3}\sigma_{kk}\delta_{ij}$ is the deviatoric Cauchy stress. The effective deviatoric stress, $\left|s_{ij}^*\right|$, is computed by [35]:

$$\left|s_{ij}^*\right| = \sqrt{\frac{3}{2}s_{ij}^*s_{ij}^*}$$

Cyclic loading of unfilled polymers will result in ratcheting or shakedown, depending on the material system and the loading properties. In theory of plasticity kinematic and isotropic hardening constitutive laws are utilized to capture the ratcheting or shakedown phenomena. Chaboche's kinematic hardening relation is given by

$$\dot{\alpha}_{ij} = \sum_{n=1}^{m}\left(\frac{2}{3}C_n\dot{\epsilon}_{ij}^p - \gamma_n\alpha_{ij}\left|\dot{\epsilon}_{ij}^p\right|\right)$$

where α_{ij} is deviatoric backstress tensor, and C_n and γ_n with $n = 1, \ldots, \mathrm{m}$ are material parameters, where we limit ourselves to $m = 2$. The yield stress σ_y is redefined as:

$$\sigma_y = \sigma_y^0 + R$$

where σ_y^0 is the initial yield strength, and R denotes the isotropic hardening effect:

$$\dot{R} = w(Q - R)|\dot{\epsilon}^p|$$

where w and Q are the material constants, and R is the accumulated amount of the incremental change of the yield surface. Then, $\sigma_y^0 + R$ represents the size of the yield surface at each cycle and R approaches to its asymptotic value through Eq. (13). It is worth noting that lifetime prediction based upon coupled cyclic plasticity-CDM models may outperform prediction techniques solely utilizing cyclic plasticity models (Chaboche, 2008; Shojaei and Wedgewood, 2017).

4.2 Fatigue damage

Microscale damage mechanisms are assumed to gradually degrade the shear and bulk moduli. The shear and bulk moduli are cyclically updated based upon state of the damage, D (following Shojaei et al., 2015):

$$\mu = \overline{\mu}(1 - D) \text{ and } K = \overline{K}(1 - D)$$

where $\overline{E}$ and $\overline{K}$ are respectively elastic and bulk moduli for the virgin polymer system, and D denotes the effective damage at each material point.

The CDM model needs to capture both low cycle fatigue (LCF) and high cycle fatigue (HCF) damage effects in which statistical models are required to account for the different failure mechanisms in LCF and HCF processes. For sake of simplicity, the rule-of-mixture is utilized to control the contribution of LCF and HCF damaging mechanisms

$$D_i = \zeta \times D_i^{LCF} + (1 - \zeta) \times D_i^{HCF}$$

where ζ is a loading characteristic and D_i^{LCF} and D_i^{HCF} denote LCF and HCF damage parameters, respectively. Following (Shojaei and Wedgewood, 2017), the loading characteristic parameter ζ is given by:

$$\zeta = \frac{(\sigma_{max} - S_e)}{(\sigma_u - S_e)}$$

where σ_u and S_e are ultimate and endurance stresses, respectively, and $S_e < \sigma_{max} < \sigma_u$ is the maximum stress in a cycle. Thus, for $\zeta = 0$ the HCF damage mechanisms dominate the fatigue failure, for $\zeta = 1$ the LCF damage mechanisms dominate the fatigue failure, and for $0 < \zeta < 1$ a linear combination of LCF and HCF damage mechanisms controls the lifetime.

The damage mechanisms in HCF correspond to initiation and propagation of microcracks and the HCF damage parameter D_i^{HCF} is defined by:

$$D_i^{HCF} = \sum_{i=1}^{3} \frac{a_i - a_0}{a_{cr} - a_0}$$

where $a_i = \int \dot{a}_i dt$ is the microcrack length that is integrated in 3 principal directions; a_0 denotes initial microcrack length, and $a_{cr} \approx 1$(mm) represents the critical crack length in which unstable fracture occurs. On the other hand, the LCF damage mechanisms are governed by void nucleation and propagation. The damage parameter for LCF is then given by:

$$D_i^{LCF} = \sum_{i=1}^{3} \frac{V - V_0}{V_{cr} - V_0}$$

where $V_i = \int \dot{V}_i dt$ is microvoid volume growth, integrated in 3 principal directions that results in an elliptical void, V_0 represents the initial microvoid volume, and $V_{cr} \approx 1\ mm^3$ represents the critical void volume in which unstable fracture occurs.

The most direct approach for calibrating the CDM fatigue model is to use directly measured S-N of E-N data to develop the constitutive laws. The main drawback is the exclusion of the computation of the self-heating and the related dependence. However, its effects are included for the frequency used to generate the data.

4.3 Implementation

The developed computational fatigue tool for engineering polymers can be implemented in commercial FEA software via user-defined material subroutines. The implementation steps are outlined in the following:

1. FEA software provides the Cauchy stress σ_{ij}, deformation gradient, F_{ij}, strain ϵ_{ij}, and strain rate strain $\dot{\epsilon}_{ij}$ for the current time step at each integration point.
2. Plastic strain increment $\delta\epsilon_{ij}^p$ is computed based on Cauchy stress σ_{ij}.
3. Microvoid volume is updated through the cycle based upon computed plastic strain ϵ_{ij}^p. Calculate the LCF damage parameter.
4. When the current cycle is completed:1
    - 4.1. Update microcrack length based on computed max stress. Calculate the HCF damage parameter.
    - 4.2. Calculate the overall damage based on LCF and HCF damage parameters
    - 4.3. Update the elastic stiffness for the next cycle computations
    - 4.4. Jump in number of cycles: $N_{next} = N_{current} + \Delta N_{jump}$.
    - 4.5. Next cycle solution is started from Step 1.

The coupling between plasticity and damage computations is enforced via cyclic updates of the elastic stiffness. The plastic deformations in subsequent cycles are influenced by the current level of fatigue damage at each integration point through the damaged stiffness.

5. Application

The performance of the developed computational platform is investigated for fatigue life prediction of Delrin® by simulating the standard fatigue test. Elastic modulus of Delrin® 100 is about 3 GPa and its Poisson's ratio is assumed 0.35. Table 1 summarizes the material model parameters for the hyperelastic-plastic CDM model.

Table 1: Hyperelastic plasticity and CDM parameters used for Delrin(r) 100

a_{cr} [mm]	a_0 [mm]	V_{cr} [mm3]	V_0 [mm3]	C_1 [MPa]	C_2 [MPa]	γ_1 [-]	γ_2 [-]	C_{10} [MPa]	C_{01} [MPa]	D_1 [MPa]
1	0	1	0	8000	800	80	5	-4600	5025.2	3000

The simulation results for cyclic loading of Delrin® 100 samples under 59, 55, and 48 MPa maximum stress (R=0.1) and f=10 Hz at room temperature are depicted in Figures 11 to 13. The coupling between CDM and hyperelastic-plastic material models results in accurate lifetime and permanent set predictions.

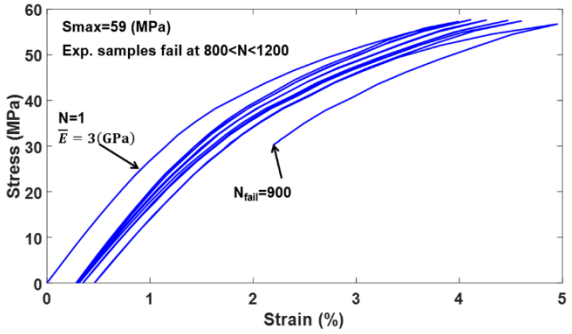

Figure 11: Hyperelastic-plastic CDM model prediction for Delrin(r) 100 at 59 MPa.

Figure 11 and 12 show the simulated stress-strain curves at different stress levels including the predicted number of cycles to failure.

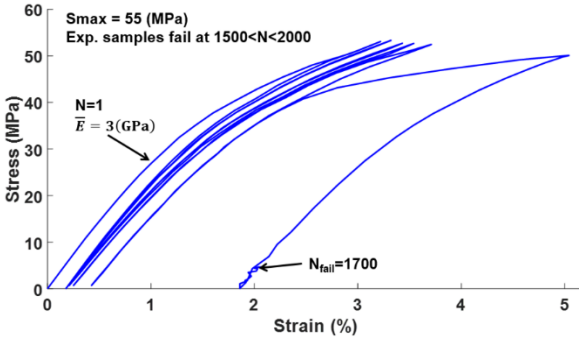

Figure 12: Hyperelastic-plastic CDM model prediction for Delrin(r) 100 at 55 MPa.

The difference in predictive performance between a standard elastic-plastic (EP) model and the hyperelastic-plastic (HEP) model described here, is shown in Figure 13 below.

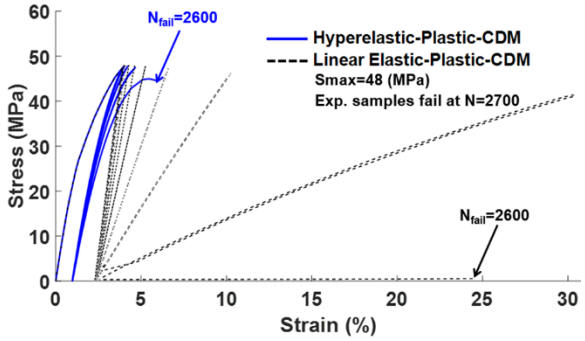

Figure 13: Difference in strain evolution prediction between EP and HEP models

The developed fatigue simulation tool performs well in capturing the experiments and provides the ability to predict low and high cycle fatigue lifetimes with acceptable accuracies. It is worth noting that the accuracy of the **lifetime predictions** is less sensitive to the elasticity and plasticity constitutive laws and is more dependent on the CDM model parameters. Since the CDM model utilizes the same SN information for both linear elastic-plastic-CDM and hyperelastic-plastic-CDM computations, the predicted lifetime for either case is expected be very close. However, the key differences are to be found in **cyclic strain response predictions** for both hyperelastic-plastic-CDM, and linear elastic-plastic-CDM models. The predicted maximum strains in the case of hyperelastic-plastic-CDM model are much closer to the experimental observations whilst the linear elastic-plastic-CDM model overpredicts the material response, as shown in Figure 14.

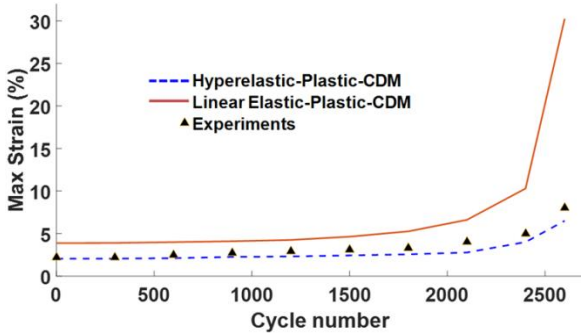

Figure 14: Maximum strain prediction for EP and HEP models

The enforced coupling between hyperelastic, plastic, and CDM models results in more accurate prediction of the progressive fatigue damage and permanent set in unfilled engineering polymers. The performance of the developed framework is compared with experimental data and it is shown that the developed framework performs well in capturing progressive permanent set, and fatigue

damage. The proposed framework can considerably increase the precision of fatigue computations in unfilled polymers and may help design engineers in their optimization tasks.

6. References

1. Chaboche, J.L., "On some modifications of kinematic hardening to improve the description of ratchetting effects", International Journal of Plasticity, Vol. 7, pp. 661-678, 1991.
2. Chaboche, J.L., "Thermodynamic formulation of constitutive equations and application to the viscoplasticity and viscoelasticity of metals and polymers", International Journal of Solids and Structures, Vol. 34(18): pp. 2239-2254, 1997.
3. Chaboche, J.L., "A review of some plasticity and viscoplasticity constitutive theories. International Journal of Plasticity", Vol. 24(10): pp. 1642-1693, 2008.
4. [38] Ghorbel, E., "A viscoplastic constitutive model for polymeric materials", Int. J. of Plasticity, Vol. 24, pp. 2032-2058, 2008.
5. Ghorbel, E., Hadriche, I., Casalino, G., Masmoudi, N., "Characterization of thermo-mechanical and fracture behaviors of thermoplastic polymers", Materials, Vol. 7, pp. 375-398, 2014
6. Maurel-Pantel, A., Baquet, E., Bikard, J., Bouvard, J.-L., Billon, N., "A thermo-mechanical large deformation constitutive model for polymers based on material network description: Application to a semi-crystalline polyamide 66", Int. J. of Plasticity, Vol. 67, pp. 102-126, 2015
7. Mooney, M., "A theory of large elastic deformation", J. of Applied Physics, Vol. 11(9), pp. 582-592, 1940.
8. Ogden, R.W., "Large deformation isotropic elasticity – on the correlation of theory and experiment for incompressible rubberlike solids", Proc. R. Soc. A: Math. Phys. Eng. Sci., Vol. 326, pp 565-584, 1972
9. Shojaei, A.K., Li, G., Tan, P.J., Fish, J., : Dynamic delamination in laminated fiber reinforced composites: a continuum damage mechanics approach", Int. J. of Solids and Structures, Vol. 71, pp. 262-276, 2015.
10. Shojaei, A.K., Wedgewood, A.R., "An anisotropic cyclic plasticity, creep and fatigue predictive tool for unfilled polymers", Mech. Mater., Vol. 106, pp. 20-34, 2017.
11. Shojaei, A.K., Volgers, P., "A coupled hyperelastic-plastic-continuum damage model for studying cyclic behavior of unfilled engineering polymers", Int. J. of Fatigue, Vol. 107, pp. 33-39, 2018.
12. Volgers, P., Winkler, A., "Analysis of DuPont Engineering Polymers – Challenges and Solutions", Science in the Age of Experience, Chicago, Il, 2017.

7. Acknowledgements

The work described in this paper could not be done without the support of many people. The authors would like to thank in particular Sergio Cosimo from the analytical laboratory in ETC,

Switzerland, James Marek and Jesse Taylor from the advanced testing laboratory and Alan Wedgewood in Wilmington (DE).

8. Disclaimer

The information provided herein corresponds to our knowledge on the subject at the date of its publication. This information may be subject to revision as new knowledge and experience becomes available. The data provided fall within the normal range of product properties and relate only to the specific material designated; these data may not be valid for such material used in combination with any other materials or additives or in any process, unless expressly indicated otherwise. The data provided should not be used to establish specification limits or used alone as the basis of design; they are not intended to substitute for any testing you may need to conduct to determine for yourself the suitability of a specific material for your particular purposes. Since DuPont cannot anticipate all variations in actual end-use conditions DuPont makes no warranties and assumes no liability in connection with any use of this information. Nothing in this publication is to be considered as a license to operate under or a recommendation to infringe any patent rights.